Analytica Chimica Acta 913 (2016) 137–144

Contents lists available at ScienceDirect

Analytica Chimica Acta

journal homepage: www.elsevier.com/locate/aca

Gold nanostar-enhanced surface plasmon resonance biosensor based on carboxyl-functionalized graphene oxide

Qiong Wu, Ying Sun, Pinyi Ma, Di Zhang, Shuo Li, Xinghua Wang, Daqian Song*

College of Chemistry, Jilin University, Qianjin Street 2699, Changchun 130012, PR China

HIGHLIGHTS

- A sensitive and versatile SPR biosensor was constructed for detection of pig IgG.
- Biofunctional gold nanostars were used to amplify the response signals.
- The strategy employed carboxyl-functionalized graphene oxide as biosensing substrate.
- The detection limit of the proposed biosensor is 32 times lower than that of graphene oxide-based biosensor.

GRAPHICAL ABSTRACT

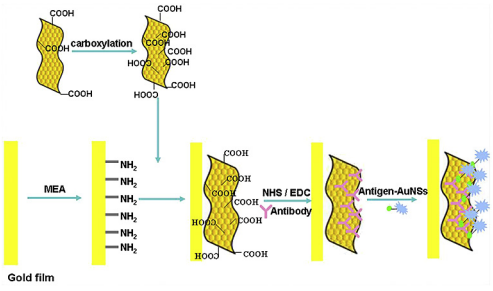

ARTICLE INFO

Article history:
Received 30 November 2015
Received in revised form
25 January 2016
Accepted 30 January 2016
Available online 4 February 2016

Keywords:
Carboxyl-functionalized graphene oxide
Gold nanostars
Surface plasmon resonance (SPR) biosensor
Pig IgG

ABSTRACT

A new high-sensitivity surface plasmon resonance (SPR) biosensor based on biofunctional gold nanostars (AuNSs) and carboxyl-functionalized graphene oxide (cGO) sheets was described. Compared with spherical gold nanoparticles (AuNPs), the anisotropic structure of AuNSs, which concentrates the electric charge density on its sharp tips, could enhance the local electromagnetic field and the electronic coupling effect significantly. cGO was obtained by a diazonium reaction of graphene oxide (GO) with 4-aminobenzoic acid. Compared with GO, cGO could immobilize more antibodies due to the abundant carboxylic groups on its surface. Testing results show that there are fairly large improvements in the analytical performance of the SPR biosensor using cGO/AuNSs-antigen conjugate, and the detection limit of the proposed biosensor is 0.0375 μg mL^{-1}, which is 32 times lower than that of graphene oxide-based biosensor.

1. Introduction

In recent years, gold nanostructure-enhanced biosensing has experienced considerable progress and played a prominent role in sensitivity enhancement of biosensors. Gold nanostructures with low toxicity, good stability and facility of surface functionalization are particularly attractive in biological applications. Plasmonic properties of gold nanostructures arise from collective oscillations of electrons in the conduction band upon irradiation, which was referred to as the localized surface plasmon resonance (LSPR) [1]. The electronic coupling between the localized surface plasmon resonance (LSPR) of gold nanostructures and the surface plasmon propagated along the surface of metallic and certain dielectric materials is often applied as a strategy to amplify the response signals of biosensors. Plasmonic properties and electromagnetic field enhancements of gold nanostructures could be tuned by controlling the size and shape of nanostructures as well as the local chemical environments [2]. Compared with smoother

* Corresponding author.
E-mail address: songdq@jlu.edu.cn (D. Song).

http://dx.doi.org/10.1016/j.aca.2016.01.063
0003-2670/

nanostructures, metallic nanoparticles with sharp tips show higher sensitivity towards refractive index changes and larger near-field enhancements [3]. The fabrication of metallic nanoparticles has seen significant progress towards morphology control and preparation of particles with sharp edges or tips, such as nanobipyramids, nanotriangles or nanostars [4,5]. Gold nanostars (AuNSs) provide tunable plasmon bands, since multiple sharp branches in their morphologies could act as 'lightning rods' and enhance the local electromagnetic fields greatly [6–8]. The plasmon peak intensities of AuNSs depend on the polarization angles of incident lights [9–11]. Applications of AuNSs for amplifying response signals of surface-enhanced Raman spectroscopy (SERS) and biosensing have been reported in several literatures [12–14].

Chemically derived GOs are atomically thin sheets of graphite that were served as precursors for graphene traditionally [15]. GO offers some advantages for optical sensing of biomolecules, including large specific surface area, good water-solubility, excellent biocompatibility and plenty of oxygen-containing functional groups. Therefore, GO-based sensing platforms were widely applied to the detection of NADH [16], TNT [17], H_2O_2 [18], dopamine [19], DNA [20], and nucleic acids [21]. The availability of several types of oxygen-containing functional groups on GO offers it the capacity for further functionalization. For instance, grassy carbon electrode modified by poly(diallyldimethylammonium chloride)-functionalized graphene oxide was used to detect quinoline yellow [22]. Graphene nanoribbons functionalized with ionic liquid were applied to the electrochemical sensing of nifedipine [23]. Amine-functionalized graphene synthesized in one step was employed for immunosensing of cardiac marker cardiac troponin I [24].

Four kinds of oxygen functionalities are known to exist in GO: epoxide (−O−), hydroxyl (−OH), carbonyl (−C═O), and carboxyl (−COOH). Epoxide and hydroxyl, located on the basal plane of GO, are the major components; carbonyl and carboxyl, distributed at the edges of GO, are the minor ones [25]. Carboxyl components could provide binding sites for many proteins, thus insufficient carboxyl groups would limit the capacity of GO to immobilize biomolecules. Therefore, increasing the ratio of carboxyl components in GO would enhance the immobilization of proteins on GO greatly.

Surface plasmon resonance (SPR) biosensors represent the mature label-free optical biosensor technology, which makes it a powerful tool for the investigation of kinetic properties of biomolecular interactions [26]. In practice, SPR biosensors were usually used to measure the changes in the refractive index on its surface, which were mainly caused by biomolecular interactions. The major drawback of routine SPR biosensor is the low sensitivity to small change in refractive index, which limits its further applications. Many researches have been conducted on the modification of the biological sensing system for enhancing sensitivity of SPR biosensors, and the key recipe could be generally summarized as the efficient immobilization of receptor and the introduction of nanomaterials for signal amplifications [21,27,28].

In this paper, a new SPR biosensor was developed based on the traditional prism-coupled SPR sensor by improving its immobilization of receptors and amplification of response signals. GO was functionalized with 4-aminobenzoic acid (PABA) to link abundant carboxyl groups and was assembled on the gold film modified by amine for immobilizing antibody. Antigen was joined with AuNSs via staphylococcal protein A (SPA) to form AuNSs-antigen conjugate. The strong electric coupling between anisotropic AuNSs and surface plasmon wave effectively promotes the changes in imaginary components of the refractive index of thin film at the chip/solution interface. Formation of conjugate also leads to change of the real component of the refractive index with the increased mass of AuNSs-antigen conjugate. Synergistic effects of cGO and AuNSs-antigen conjugate contribute to the significant sensitivity enhancement of the sensor response.

2. Materials and methods

2.1. Reagents and materials

Pig IgG, rabbit anti-pig IgG, human IgG, and bovine IgG were purchased from Beijing Biosynthesis Biotechnology Company. Bovine serum albumin (BSA) was purchased from Ding Guo Biotechnology Company. Chicken serum was purchased from Shanghai Jonln Industrial Company. Graphite was purchased from Sigma–Aldrich. Staphylococcal protein A (SPA), 2-mercaptoethylamine (MEA), 1-ethyl-3-(3-dimethylaminopropyl) carbodiimide (EDC) and N-hydroxysuccinimide (NHS) were purchased from Jkchemical. Hydrogen tetrachloroauratehydrate ($HAuCl_4 \cdot 3H_2O$) was purchased from Acros. 4-aminobenzoic acid (PABA), nitric acid, sodium nitrite, silver nitrate, ascorbic acid, hydrogen peroxide, sodium hydroxide, sodium citrate, hydrochloric acid, and ethanol were purchased from Sinopharm Chemical Reagent Co., Ltd. All chemicals were of analytical grade and used without further purification. Deionized water (DI-water) was prepared using a Millipore purification device.

Rabbit anti-pig IgG, pig IgG, human IgG and bovine IgG were stored at −20 °C and all biological reagents were stored at 4 °C. Sodium phosphate buffered saline (PBS, 0.01 mol L^{-1}, pH 7.4) was used as the running buffer.

2.2. Equipment

A wavelength modulation SPR biosensor developed by our research group was used. It consists of an iodine-tungsten lamp, a light guide system, a prism-sensing unit, a flow cell reactor, a miniature spectrometer and a data-processing system. Kretschmann configuration was applied in the sensing unit to achieve the surface plasmon resonance through attenuated total reflection at the interface between a prism and a thin metal layer. A gold film coated on a glass slide was fixed on the surface of an optical prism by using suitable index-matching oil. The transverse-magnetic polarized parallel light, where was obtained by modulating the excitation light emitted from the iodine-tungsten lamp with an optical collimator combined with a polarizer, was streaming to the interface between the gold film and the sample solution to excite surface plasmons, after passing through one side of the prism. The output light from another side of the prism was guided to the miniature spectrometer by using a focusing optical lens. The miniature spectrometer (HR2000+, Ocean Optics Inc., USA) employed in this work consists of a high-resolution optical grating, a 2-MHz analog-to digital converter, a 2048-element linear charge coupled device (CCD) detector and a high-speed USB 2.0 interface. By using the proposed SPR biosensor, the observed resonant wavelength shifts respond to the interactions between the biomolecules immobilized on the biosensor and the analytes dissolved in solution.

Transmission electron microscopy (TEM) images of AuNSs and AuNPs were taken using a Hitachi H800 transmission electron microscope (Hitachi Ltd., Japan) operating at 200 kV. Atomic force microscopy (AFM) images of GO were obtained on a Nanoscope III scanning probe microscope (Digital Instruments) in tapping mode under ambient conditions. Scanning electron microscope (SEM) images of the biosensor were taken using a Hitachi SU8020 scanning electron microscope (Hitachi Ltd., Japan) operating at 3 kV. UV–Vis absorption spectra of the AuNSs and AuNPs were recorded on a TU-1810C UV–Vis spectrometer (Beijing Purkinje General

Instrument Co., Ltd.). X-ray photoelectron spectroscopy (XPS) analysis was performed using a R3000/Vuv5k/Mx-650 spectrometer (Prevac) equipped with a monochromatized Al Kα (1486.7 eV) X-ray source.

2.3. Synthesis of GO and cGO

GO was prepared using the modified Hummers and Offeman's method from graphite powders [29]. cGO was acquired by functionalizing GO with PABA based on the diazonium reaction [30]. The formation of cGO was demonstrated by AFM and XPS analysis.

2.4. Conjugation of antigen and gold nanostructures

A simple and surfactant-free method was adopted to prepare high-yield monodisperse gold nanostars [31]. Briefly, the seed solution was prepared by adding 15 mL of 1% citrate solution to 100 mL of boiling 1 mM $HAuCl_4$ solution under vigorous stirring. After boiling for 15 min, the solution was cooled and filtered by a 0.22 μm nitrocellulose membrane. For nanostar synthesis, 300 μL of the above citrate-stabilized seed solution was added into 30 mL of 0.25 mM $HAuCl_4$ solution (with 30 μL of 1 M HCl) at room temperature under moderate stirring (700 rpm). Then, 300 μL of 1 mM silver nitrate ($AgNO_3$) and 150 μL of 100 mM ascorbic acid (AA) were added simultaneously. The mixed solution was stirred for 30 s and its color rapidly turned from light red to blue or greenish-black. Immediately afterwards, the centrifugation step at 8000 rpm for 15 min was carried out to halt the nucleation. The precipitate was redispersed in DI-water, filtered by a 0.22 μm nitrocellulose membrane, and then kept at 4 °C for long-term storage. Subsequently, 50 μL of SPA (1 mg mL^{-1}) was added to 450 μL of PBS containing AuNSs followed by gently shaking for several seconds. The mixture was kept for 3 h at 4 °C in order to wrap the AuNSs with SPA and then was centrifuged to remove excess SPA in supernatant. The precipitate was re-dispersed in PBS and antigen (pig IgG) was added. The mixture with the volume adjusted to 500 μL by using PBS was stood overnight at 4 °C and pig IgG could be steadily adhered to AuNSs via strong integrating force between SPA and pig IgG. To validate the formed AuNSs-antigen conjugate, UV–Vis spectroscopy was applied to detect the change of localized surface plasmon before and after the conjugate reaction of antigen and gold nanostructures. Prior to the analysis, 10 μL of 10 mg mL^{-1} BSA was employed to block the nonbinding sites of AuNSs. AuNPs were prepared by a classic method [32]. AuNPs-antigen conjugate was fabricated and tested by the same procedure mentioned above.

2.5. Preparation of sensing substrate based on GO and cGO

The glass slide coated with gold film was fixed in the bottom of the reactor to form a flow chamber. PBS was firstly injected into the reactor to balance the baseline of SPR signals, and then 10 mM MEA was injected into the reactor followed by incubating for 1 h to link abundant amino groups on the surface of the gold film. Subsequently, 1 mg mL^{-1} cGO was injected into the reactor and cGO was assembled on the gold film via electrostatic interaction. After 60 min, the mixture of NHS/EDC (1.5 mM, 7.5 mM) was introduced to activate the carboxyl groups of cGO. 20 min later, PBS was employed again to wash off the excess NHS/EDC and balance the baseline of SPR signals. When the shift of the resonant wavelength was unchanged, rabbit anti-pig IgG (antibody) was injected into the reactor to covalently attach to the activated cGO surfaces. After 12 h, PBS buffer was injected to wash off the unbound antibody and stabilize the baseline of SPR signals. Prior to analysis, 1 mol L^{-1} ethanolamine hydrochloride (pH 8.0) was served as sealant to block the non-specific binding sites of cGO. The sensing substrate based on GO was prepared by the same procedure.

2.6. Immunoassay

The pig IgG solution at a certain concentration level was injected into the reactor and the resonant wavelength shift was recorded in real time at room temperature. The specific reaction between pig IgG and rabbit anti-pig IgG could be completed within 40 min. Then, PBS was injected to dissociate the antigen from the antibody. When the resonant wavelength shifted back to the original position, another sample solution was sequentially injected into the reactor for measurement. Analogously, AuNSs-antigen and AuNPs-antigen conjugates were determined. All experiments were conducted in triplicate. Schematic illustration of the assay procedure is shown in Fig. 1. The specificity of the proposed biosensor was confirmed via determining human IgG and bovine IgG by the same procedure described above.

3. Results and discussions

3.1. Characterization of cGO, AuNP and AuNS

XPS was used to analyze the compositions of GO and cGO. The C/O atomic ratio in GO and cGO was 1.86 and 2.99 (Table 1), respectively. The higher C/O atomic ratio in cGO indicates that benzoic acid, whose C/O atomic ratio is 3.5, is immobilized on the surface of GO. Furthermore, the high-resolution analyses of O1s spectra shown in Fig. 2A and B convincingly demonstrate the connection of the benzoic group onto GO surface. The connection could not be verified by the analyses of C1s spectra because the signals of C–C bonds from benzene rings increase along with the increase of the signals of C=O bonds from carboxyl groups. Therefore, it is difficult to evaluate the diazonium reaction in terms of C1s peaks in XPS spectra. However, the signals of oxygen from carboxyl groups in O1s spectra could be taken as the indicator of the diazonium reaction since all the oxygen atoms were in forms of carboxyl groups. Three major peaks located at 530.8 eV, 532.3 eV, and 534.2 eV in O1s spectra were assigned to Ar–C(O)–OH, Ar–C(O)–OH, and C–OH-(aromatic), in which Ar denoted aromatic carbon and the contributing oxygen atoms were underlined [33–35] (Fig. 2A and B). The peak energies and the corresponding atomic percentages are listed in Table 2. After GO reacted with PABA, carboxyl groups offered all the oxygen atoms, which led to the increase of atomic-percentages of Ar–C(O)–OH from 68.5% to 86.2% and the decrease of atomic-percentages of C–OH from 23.6% to 3.1%. The results clearly indicate that considerable amounts of carboxyl groups were attached to the surface of GO, which could be employed for further immobilization of biomolecules. The exfoliated cGO sheets were measured to be about 0.963 nm thick by AFM (Fig. S1), which is in close proximity to the thickness of single layered GO sheets [36]. There is no noticeable difference on the morphology of GO and cGO in AFM images.

TEM images of AuNPs and AuNSs are shown respectively in the inset of Fig. 3A and B. Uniform AuNPs with an average diameter of 25 nm without aggregation are shown in TEM image. The synthesis of surfactant-free AuNSs is extremely simple and the reaction could be completed in 30 s at room temperature. The size distribution of the prepared AuNSs is narrow. Each AuNS particle has five or more tips, and the mean values of core diameters, branch lengths and tip diameters of which are 27 nm, 12 nm and 9 nm, respectively. UV–Vis absorption spectra of AuNPs and AuNSs before and after antigen conjugation in Fig. 3A and B shows red shifts of 9 nm and 20 nm respectively. These shifts demonstrate the formation of AuNPs-antigen and AuNSs-antigen conjugate via the linkage of SPA. Moreover, the red shifts of resonant wavelength imply the

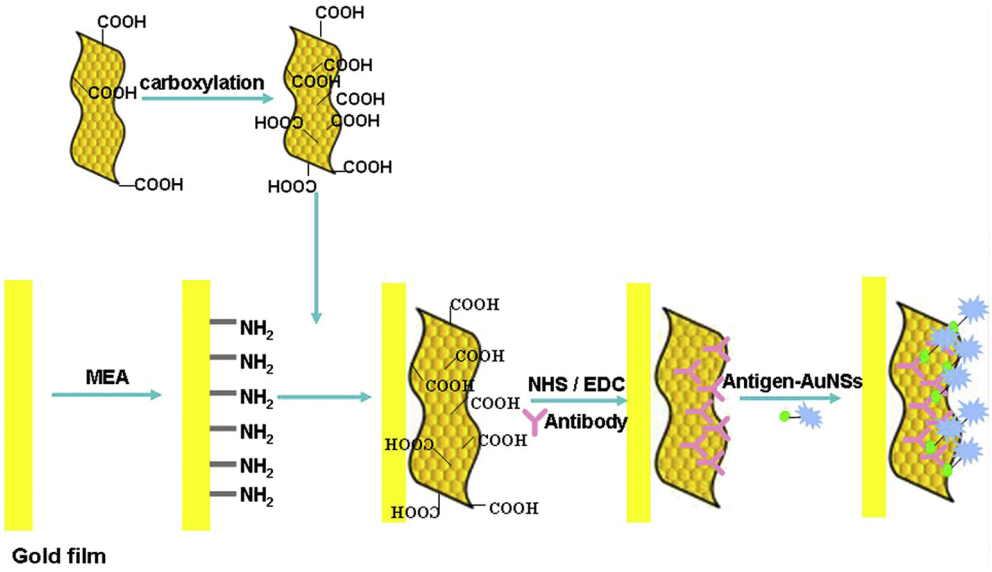

Fig. 1. Schematic diagram of experimental procedure. (Y) antibody (), antigen-AuNSs (), antigen-AuNPs (), GO sheets (), cGO sheets.

Table 1
Atomic percentage of major elements in GO and functionalized GO obtained by XPS. Unconcerned trace elements were neglected.

	GO	cGO
C (%)	65.03	74.92
O (%)	34.97	25.08

Table 2
Analysis of O1s binding energies and atomic percentage of oxygens in different chemical states of GO and cGO.

	Ar–C(O)–OH (530.8 eV) (%)	Ar–C(O)–OH (532.3 eV) (%)	C–OH (aromatic) (534.2 eV) (%)
GO	7.9	68.5	23.6
cGO	10.7	86.2	3.1

difference in sensitivity between the two nanoparticles to changes in surroundings associated with coating additional molecular layers.

3.2. Antibody biochip based on GO and cGO

GO and cGO were separately assembled on gold film for the future immobilization of antibodies. MEA was employed as the bridging agent since its thiol group have a strong affinity to the gold film surface and the opposite amine group, which is positively charged, could adsorb GO and cGO via electrostatic interaction. Self-assembling processes of GO and cGO on gold films could be completed in 1 h, resulting in the resonant wavelength shifts of 6.0 nm and 9.7 nm, respectively (Fig. S2). The difference of the resonant wavelength shifts indicates the introduction of benzoic acid on cGO is beneficial to its assembly on gold film. The real-time measurements of resonant wavelengths after the assembling of GO or cGO sheets on amino-modified gold films showed that there was few change of resonant wavelength during 24 h, indicating that the assembling was stable enough for the following experiment. The carboxylic groups on cGO sheets were further activated with EDC/NHS.

To optimize the concentration of antibody for immobilization, resonant wavelength shifts were measured by injecting gradient

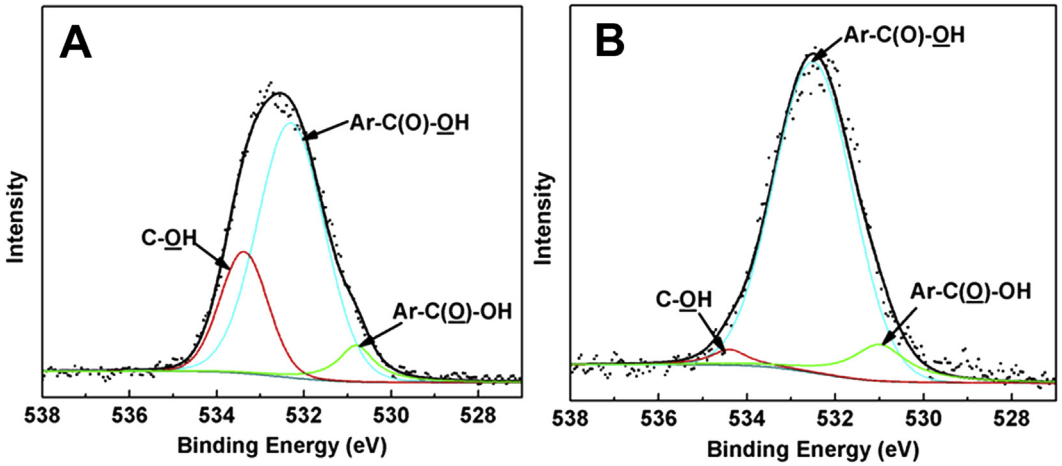

Fig. 2. XPS O1s spectra of GO (A) and cGO (B).

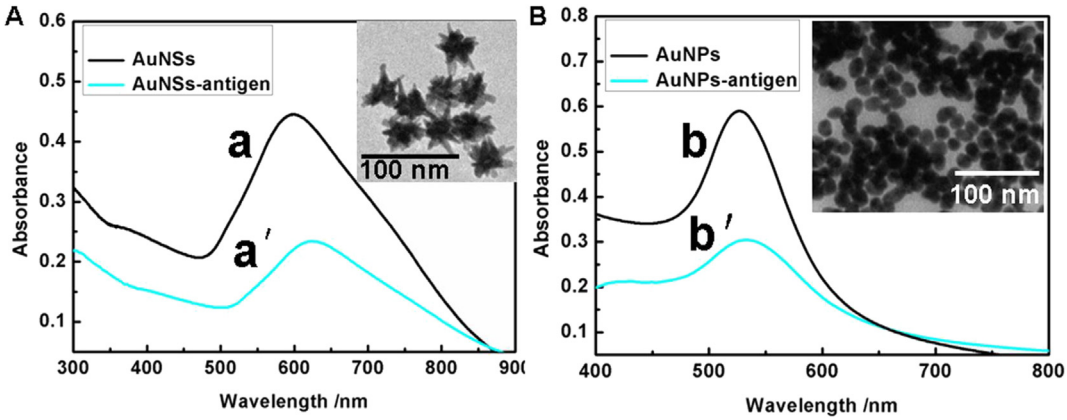

Fig. 3. UV–Vis absorption spectra of AuNSs (a), AuNSs-antigen (a′), AuNPs (b) and AuNPs-antigen (b′). Inset shows TEM images of AuNSs (A) and AuNPs (B).

concentrations of antibody into the reactor. As shown in Fig. 4, resonant wavelength gradually moves to longer wavelength with the increase of antibody concentrations. Resonant wavelength shift reaches a maximum when the antibody immobilized on the surface GO or cGO reaches saturation. The optimal antibody concentration for GO is 100 μg mL^{-1} and the maximum resonant wavelength is 11.2 nm (Fig. 4A). When cGO was used, the shift of resonant wavelength attains its maximum with injecting 100 μg mL^{-1} antibody and the maximum of resonant wavelength shift is 15.3 nm (Fig. 4B). Since the resonant wavelength shifts increase with the amount increase of antibody immobilized on the sensor surface, cGO sheets could load more antibody compared with GO sheets, which indicates that abundant carboxyl groups of cGO lead to larger capacity for immobilization of antibody. Therefore, cGO demonstrates a great potential in fabricating biosensors for its obvious capacity of loading antibody or other biomolecules.

3.3. GO and cGO based SPR biosensor for immunoassay

The performance of sensors based on GO and cGO were evaluated and the results were shown in Fig. 5. The minimum resonant wavelength shift that could be detected with the SPR biosensor installed in our laboratory is 0.20 nm, which determines the lowest detection concentration of the antigen. The SPR biosensors based on GO and cGO show good responses to pig IgG in the concentration ranges of 1.25–40 μg mL^{-1} and 0.6–40 μg mL^{-1}, with the corresponding resonant wavelength shifts of 0.20–3.2 nm and 0.20–5.8 nm, respectively.

3.4. Optimization of gold nanostructures-enhanced SPR sensing

Spiky nanoparticles have been demonstrated to have high sensitivity towards refractive index changes and large near field enhancement in theory and practice [37]. Therefore, AuNSs with protruding sharps were anticipated to be an excellent candidate in sensitivity enhancement for biological applications. In this paper, a

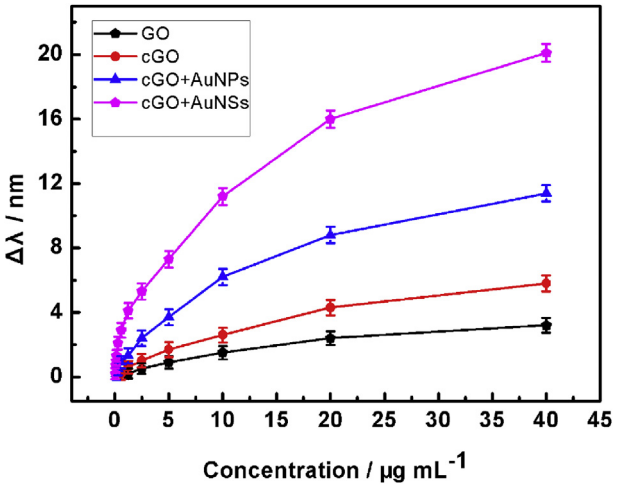

Fig. 5. Relationships between concentrations of pig IgG and shifts of resonant wavelengths obtained with biosensors based on GO, cGO, cGO/AuNPs-antigen and cGO/AuNSs-antigen conjugate.

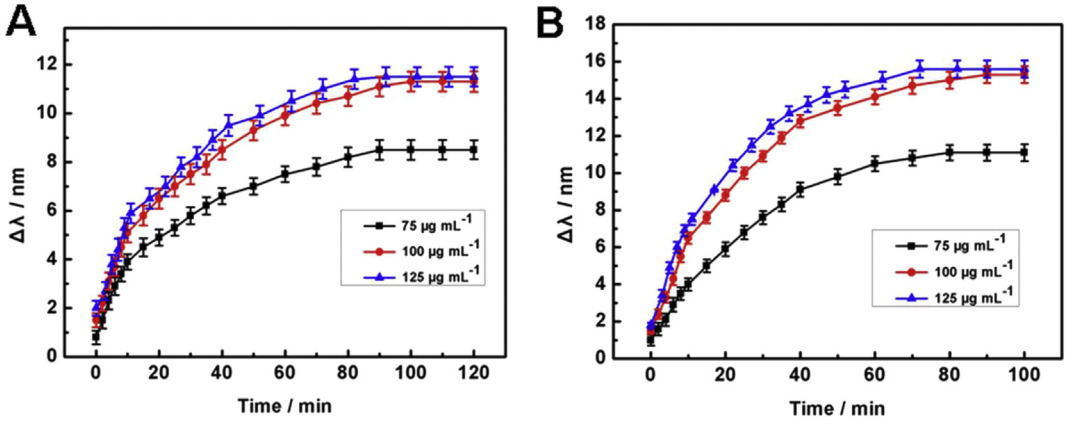

Fig. 4. Kinetic adsorption curves of rabbit anti-pig IgG at different concentrations on GO-modified gold film (A) and cGO-modified gold film (B).

novel, surfactant-free synthesis method was adopted to prepare biocompatible AuNSs. Traditional refractive-index-based biosensing utilizing AuNSs remains limited because the shift in plasmon resonance from a bulk solution of AuNSs, upon additions of analytes, is commonly slight. The reason is that the AuNSs are routinely synthesized using polyvinylpyrrolidone (PVP) as the capping agent, it is feasible that PVP prevents analytes from the binding to the surface of AuNS [38]. The surfactant-free synthesis makes AuNSs accessible to directly bind molecules which could interact with gold.

To prove the multiple sharp branches of AuNSs greatly enhance the local electromagnetic field, AuNPs with the similar size to the core of AuNSs were prepared for comparison. Prior to comparison of the SPR signals obtained with the two nanostructure-antigen conjugates, the ratios between antigens and nanostructures were optimized by analyzing sample solutions with uniform concentration of antigen using the cGO-based SPR biosensor. The effect of the volume of AuNSs colloid is shown in Fig. 6. SPR signals firstly increases rapidly and then trends to stabilize with the increase of the volume of AuNSs colloid. The result implies AuNSs bound on gold film reaches saturation when the volume of AuNSs colloid is 150 μL. Therefore, 150 μL of as-prepared AuNSs solution was selected as the optimum volume to form AuNSs-antigen conjugate. By the same procedure, 120 μL of as-prepared AuNPs solution was selected as the optimum volume to form AuNPs-antigen conjugate.

3.5. Gold nanostructures-enhanced SPR biosensor based on cGO for immunoassay

A series of repeat experiments were performed by varying the concentration of antigen to evaluate the performance of the developed SPR biosensors based on cGO as sensing substrate and AuNSs-antigen or AuNPs-antigen conjugate as signal enhancer. After the AuNSs-antigen conjugates with the antigen concentration of 20 μg mL^{-1} were injected into the reactor for immunoassay, the SEM image (Fig. 7) of the biosensor was taken. As can be observed in Fig. 7, AuNSs distributed on cGO sheets. The analytical performances of the biosensor used in this study were shown in Fig. 5. The developed SPR biosensor based on cGO/AuNSs-antigen conjugate shows a sensitive response to pig IgG in the concentration range of 0.0375–40 μg mL^{-1}, with the minimum and maximum shifts of resonant wavelength of 0.20 nm and 20.6 nm, respectively. The association constant of pig IgG with antibody is calculated to be 5.82×10^7 L mol^{-1}. The SPR biosensor based on cGO/AuNPs-antigen conjugate shows a good response to pig IgG in the concentration range of 0.150–40 μg mL^{-1}, with the minimum and maximum shifts of resonant wavelength of 0.20 nm and 11.4 nm, respectively. The association constant of pig IgG with antibody is calculated to be 3.46×10^7 L mol^{-1}. Under same experimental conditions, the lowest concentration that could be detected with the biosensor based on cGO/AuNSs-antigen conjugate is 0.0375 μg mL^{-1}, which is 4 times lower than that obtained with the biosensor based on cGO/AuNPs-antigen conjugates, 16 times lower than that obtained with the cGO-based biosensor and 32 times lower than that obtained with the GO-based biosensor. Additionally, a comparison between the proposed immunosensor and previously reported immunosensors for IgG were also made (Table 3). It can be seen that the proposed immunosensor could provide both satisfactory detection limit and wide detection range.

Consequently, the signal enhancements of SPR biosensors obtained by introducing gold nanostructures might originate from the changes in the real and imaginary components of the refractive index of the thin film at the chip/solution interface. Introduction of high-density gold nanostructures increases the mass of analyte adhered to the sensing film could affect the real component value. Near-field electronic coupling between AuNSs and the surface plasmon wave primarily affects the imaginary component. Anisotropic structures of AuNSs could concentrate the electric field around the sharp tips more effectively than isotropic AuNPs, because of the lightning rod effect [39,40]. In the developed SPR biosensor, pig IgG conjugated with AuNSs was exposed to rabbit anti-pig IgG immobilized on the surface of cGO. AuNSs with protuberant sharps induce strong local electromagnetic fields and exhibit stronger amplification of response signals originating from the binding of antigen to antibody than AuNPs. The experimental results indicate that the antigen-labeled AuNSs is a powerful tool for the amplification of SPR response signals.

Carboxyl-functionalized GO not only could be applied to overcome the limits of the sites for immobilizing proteins in GO by increasing the active carboxylic groups, but also retains all advantages of GO for optical sensing of biomolecules. The remarkable improvement of cGO for immobilizing antibody has been proved by experiments in this work, which leads to the sensitivity enhancement in subsequent immunoassays. As cGO could be easily transformed from GO, it becomes a promising alternative to be widely used in immunoassays.

Meanwhile, the detection of human IgG and bovine IgG under the same experimental conditions mentioned above was

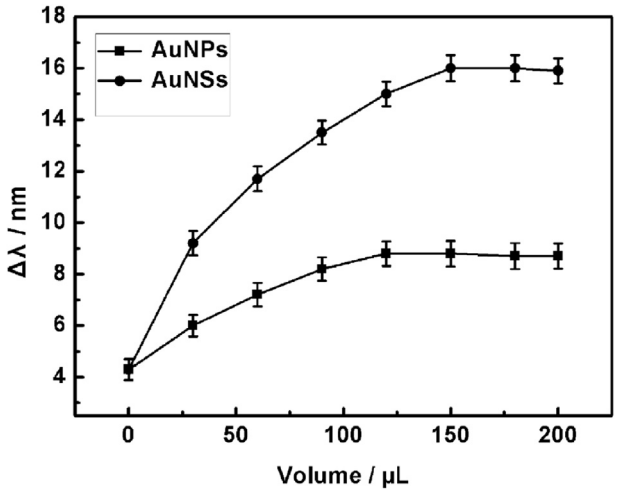

Fig. 6. Relationship between shifts of resonant wavelengths and volumes of AuNPs and AuNSs colloids. Concentration of pig IgG is 20 μg mL^{-1}.

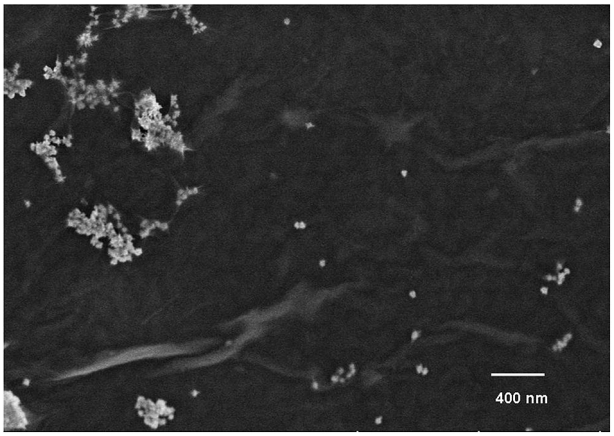

Fig. 7. SEM image of the proposed biosensor.

Table 3
Comparison of analytical performances with other reported immunosensors.

Immunosensor	Detection range (μg/mL)	Detection limit (μg/mL)	References
Rabbit anti-pig IgG/cGO/Au nanostars	0.0375–40	0.0375	Present work
Rabbit anti-bovine IgG/triangular Ag nanoplates/chitosan	0.075–40	0.075	[41]
Biotinylated anti-human IgG/Polyaniline–silicon	5–550	5	[42]
Anti-human IgG/$CdFe_2O_4$–SiO_2/CPE	0.51–30.17	0.18	[43]
rabbit anti-dog IgG/COOH–Fe_3O_4/Ag/Au	0.15–40	0.15	[44]
Goat anti-human IgG/Au–graphene oxide	0.1–50	0.1	[45]
Goat anti-human IgG/polydopamine	2–100	0.9	[46]
Goat anti-human IgG/COOH–MWCNT/Fe_3O_4	0.03–1	0.025	[47]

performed to evaluate the specificity of SPR biosensor based on cGO and AuNSs-antigen conjugate. After rabbit anti-pig IgG was immobilized on activated cGO sheets, AuNSs-human IgG and AuNSs-bovine IgG conjugates at the IgG concentration of

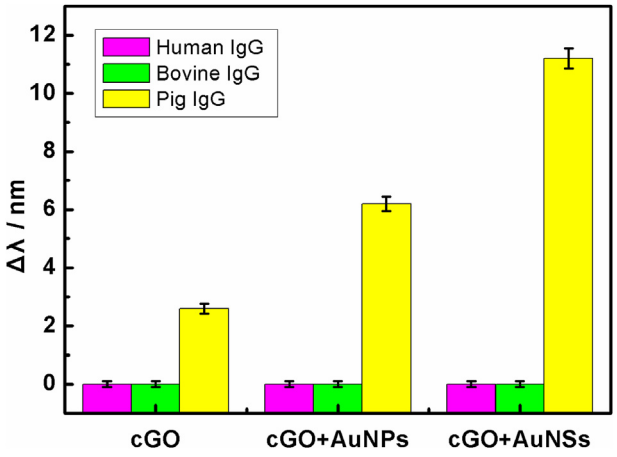

Fig. 8. Shifts of resonant wavelengths obtained for different antigens by using SPR biosensors based on cGO, cGO/AuNPs-antigen and cGO/AuNSs-antigen conjugate.

10 μg mL^{-1} were injected separately into the reactor for immunoassay. The results (Fig. 8) show that the resonant wavelengths was almost unchanged, which presents that the proposed SPR biosensor has the ability of selective detection of pig IgG.

3.6. Analysis of real samples

In order to validate the excellent specificity and high sensitivity of the proposed biosensor for the detection of pig IgG, recovery experiments were performed using chicken serum. Chicken serums were separately spiked with the pig IgG standard solutions at three different concentrations levels, and then, the spiked serum samples were directly determined by the proposed biosensor. Prior to the detection, the volume of the AuNSs should be re-optimized due to the unwanted adsorption of proteins in serum to the surfaces of SPA-modified AuNSs. The procedure of the re-optimization was similar with that mentioned above and the obtained optimal volume of AuNSs added in serum was 210 μL. Under the optimal conditions, the chicken serum samples with the spiked levels of pig IgG at 5, 10, 20 μg mL^{-1} were analyzed by the proposed biosensor. As reference, the PBS solutions with the same spiked levels of pig IgG were also analyzed. The results were listed at Table 4. The recovery of the present method was between 103% and 106%, which suggested that the non-specific interactions induced by the serum matrix could be negligible, and the proposed biosensor was available for determining pig IgG in real serum samples.

Table 4
Analytical results of pig IgG in chicken serum (n = 3).

Content of pig IgG (μg/mL)	Spiked (μg/mL)	Shifts in PBS (nm)	Shifts in serum (nm)	Recovery (%)
None	5	7.3	7.7	105.5
None	10	11.2	11.6	103.6
None	20	16.0	16.5	103.1

4. Conclusion

In this paper, a novel design for the fabrication of a sensitive SPR biosensor was demonstrated. Carboxyl-functionalized GO was introduced into the developed biosensor due to its superior ability of immobilizing antibodies originated from the abundant carboxylic groups on its surface, and was validated by the comparison with the routine GO. The performances of AuNSs and AuNPs for the SPR signal enhancements were evaluated by the detection of pig IgG under the optimal experimental conditions. The developed SPR biosensor based on cGO/AuNSs-antigen conjugate shows a sensitive response to pig IgG in the concentration range of 0.0375–40 μg mL^{-1}. The combination of cGO and AuNSs, which could be adopted for the detection of various proteins by changing the corresponding receptors, offers a new strategy for the construction of SPR biosensors.

Acknowledgments

This work was supported by Special-funded Programme on National Key Scientific Instruments and Equipment Development of China (No. 2012YQ090194), National Natural Science Foundation of China (Nos. 21207047 and 21405057), and Science and Technology Developing Foundation of Jilin Province (Nos. 20150311099YY, 20121808 and 20150204017YY).

Appendix A. Supplementary data

Supplementary data related to this article can be found at http://dx.doi.org/10.1016/j.aca.2016.01.063.

References

[1] K.A. Willets, R.P. Van Duyne, Localized surface plasmon resonance spectroscopy and sensing, Annu. Rev. Phys. Chem. 58 (2007) 267–297.
[2] K.L. Kelly, E. Coronado, L.L. Zhao, G.C. Schatz, The optical properties of metal nanoparticles: the influence of size, shape, and dielectric environment, J. Phys. Chem. B 107 (2003) 668–677.
[3] A. Shiohara, J. Langer, L. Polavarapu, L.M. LizMarzan, Solution processed polydimethylsiloxane/gold nanostar flexible substrates for plasmonic sensing, Nanoscale 6 (2014) 9817–9823.
[4] M.R. Langille, M.L. Personick, J. Zhang, C.A. Mirkin, Defining rules for the shape evolution of gold nanoparticles, J. Am. Chem. Soc. 134 (2012) 14542–14554.
[5] J.R.G. Navarro, D. Manchon, F. Lerouge, N.P. Blanchard, S. Marotte, Y. Leverrier, J. Marvel, F. Chaput, G. Micouin, A. Gabudean, A. Mosset, E. Cottancin, P.L. Baldeck, K. Kamada, S. Parola, Synthesis of PEGylated gold nanostars and bipyramids for intracellular uptake, Nanotechnology 46 (2012) 465602–465609.
[6] C.M. Cobley, L. Au, J.Y. Chen, Y.N. Xia, Targeting gold nanocages to cancer cells for photothermal destruction and drug delivery, Expert Opin. Drug. Del. 7 (2010) 577–587.
[7] D.H.M. Dam, J.H. Lee, P.N. Sisco, D.T. Co, M. Zhang, M.R. Wasielewski,

T.W. Odom, Direct observation of nanoparticle-cancer cell nucleus interactions, ACS Nano 6 (2012) 3318–3326.
[8] J.N. Anker, W.P. Hall, O. Lyandres, N.C. Shah, J. Zhao, R.P. Van Duyne, Biosensing with plasmonic nanosensors, Nat. Mater. 7 (2008) 442–453.
[9] O. Bar-Ilan, R.M. Albrecht, V.E. Fako, D.Y. Furgeson, Toxicity assessments of multisized gold and silver nanoparticles in zebrafish embryos, Small 5 (2009) 1897–1910.
[10] L. Rodriguez-Lorenzo, R.A. Alvarez-Puebla, I. Pastoriza-Santos, S. Mazzucco, O. Stephan, M. Kociak, L.M. Liz-Marzan, F.J.G. Abajo, Zeptomol detection through controlled ultrasensitive surface-enhanced Raman scattering, J. Am. Chem. Soc. 131 (2009) 4616–4618.
[11] L. Rodriguez-Lorenzo, R. Rica, R.A. Alvarez-Puebla, L.M. LizMarzan, M.M. Stevens, Plasmonic nanosensors with inverse sensitivity by means of enzymeguided crystal growth, Nat. Mater. 11 (2012) 604–607.
[12] A.H. Nguyen, X.Y. Ma, S.J. Sim, Gold nanostar based biosensor detects epigenetic alterations on promoter of real cells, Biosens. Bioelectron. 66 (2015) 497–503.
[13] Y.S. Wang, L. Polavarapu, L.M. Liz-Marzan, Reduced graphene oxide-supported gold nanostars for improved SERS sensing and drug delivery, ACS Appl. Mater. Interfaces 6 (2014) 21798–21805.
[14] X.W. Cao, C.W. Shi, W.B. Lu, H. Zhao, M. Wang, W. Tong, J. Dong, X.D. Han, W.P. Qian, Synthesis of Au nanostars and their application as surface enhanced Raman scattering-activity tags inside living cells, Nanosci. Nanotechnol. 15 (2015) 4829–4836.
[15] A. Bagri, C. Mattevi, M. Acik, Y.J. Chabal, M. Chhowalla, V.B. Shenoy, Structural evolution during the reduction of chemically derived graphene oxide, Nat. Chem. 2 (2010) 581–587.
[16] M. Govindhan, M. Amiri, A. Chen, Au nanoparticle/graphene nanocomposite as a platform for the sensitive detection of NADH in human urine, Biosens. Bioelectron. 66 (2015) 474–480.
[17] Q. Zhang, D.M. Zhang, Y.L. Lu, Y. Yao, S. Li, Q.J. Liu, Graphene oxide-based optical biosensor functionalized with peptides for explosive detection, Biosens. Bioelectron. 68 (2015) 494–499.
[18] C.M. Yu, L. Wang, W.B. Li, C. Zhu, N. Bao, H.Y. Gu, Detection of cellular H_2O_2 in living cells based on horseradish peroxidase at the interface of Au nanoparticles decorated graphene oxide, Sens. Actuator B-Chem. 211 (2015) 17–24.
[19] X.H. Wang, F.F. Zhang, J.F. Xia, Z.H. Wang, S. Bi, L. Xia, Y.H. Li, Y.Z. Xia, L.H. Xia, Modification of electrode surface with covalently functionalized graphene oxide by L-tyrosine for determination of dopamine, J. Electroanal. Chem. 738 (2015) 203–208.
[20] X. Huang, X.P. Huang, A. Zhang, B.G. Zhuo, F.S. Lu, Y.W. Chen, W.H. Gao, Quenching of the electrochemiluminescence of RU-complex tagged shared-stem hairpin probes by graphene oxide and its application to quantitative turn-on detection of DNA, Biosens. Bioelectron. 70 (2015) 441–446.
[21] R. Li, F. Feng, Z.Z. Chen, Y.F. Bai, F.F. Guo, F.Y. Wu, G. Zhou, Graphene oxide-assisted nucleic acids assays using conjugated polyelectrolytes-based fluorescent signal transduction, Talanta 140 (2015) 143–149.
[22] L. Fu, Y.H. Zheng, A.W. Wang, W. Cai, H.T. Lin, Sensitive determination of quinoline yellow using poly (diallyldimethylammonium chloride) functionalized reduced graphene oxide modified grassy carbon electrode, Food Chem. 181 (2015) 127–132.
[23] L. Shang, F.Q. Zhao, B.Z. Zeng, Highly dispersive hollow PdAg alloy nanoparticles modified ionic liquid functionalized graphene nanoribbons for electrochemical sensing of nifedipine, Electrochim. Acta 168 (2015) 330–336.
[24] S.K. Tuteja, M. Kukkar, C.R. Suri, A.K. Paul, A. Deep, One step in-situ synthesis of amine functionalized graphene for immunosensing of cardiac marker cTnI, Biosens. Bioelectron. 66 (2015) 129–135.
[25] X.F. Gao, J.Y. Jang, S.J. Nagase, Hydrazine and thermal reduction of graphene oxide: reaction mechanisms, product structures, and reaction design, J. Phys. Chem. C 114 (2010) 832–842.
[26] H. Sipova, J.R. Homola, Surface plasmon resonance sensing of nucleic acids: a review, Anal. Chim. Acta 773 (2013) 9–23.
[27] X.W. Guo, Fe3O4@Au nanoparticles enhanced surface plasmon resonance for ultrasensitive immunoassay, Sens. Actuator B Chem. 205 (2014) 276–280.
[28] C. Huttl, C. Hettrich, M. Riedel, P. Henklein, H. Raweland, F.F. Bier, Development of peptidyl lysine dendrons: 1,3-dipolar cycloaddition for peptide coupling and antibody recognition, Chem. Biol. Drug Des. 85 (2015) 565–573.
[29] L.J. Cote, F. Kim, J.X. Huang, Langmuir-blodgett assembly of graphite oxide single Layers, J. Am. Chem. Soc. 131 (2009) 1043–1049.
[30] H.Y. Zhang, Z.F. Li, A. Snyder, J. Xie, L.A. Stanciu, Functionalized graphene oxide for the fabrication of paraoxon biosensors, Anal. Chim. Acta 827 (2014) 86–94.
[31] H. Yuan, C.G. Khoury, H.J. Wang, C.M. Wilson, G.A. Grant, T. Vo-Dinh, Gold nanostars: surfactant-free synthesis, 3D modelling, and two-photon photoluminescence imaging, Nanotechnology 23 (2012) 075102–075110.
[32] G. Frens, Controlled nucleation for the regulation of the particle Size in monodisperse gold suspensions, Nat. Phys. Sci. 241 (1973) 20–22.
[33] D. Briggs, G. Beamson, XPS studies of the oxygen 1s and 2s levels in a wide range of functional polymers, Anal. Chem. 65 (1993) 1517–1523.
[34] S.H. Shim, K.T. Kim, J.U. Lee, W.H. Jo, Facile method to functionalize graphene oxide and its application to poly(ethylene terephthalate)/graphene composite, ACS Appl. Mater. Inter. 4 (2012) 4184–4191.
[35] A. Ganguly, S. Sharma, P. Papakonstantinou, J. Hamilton, Probing the thermal deoxygenation of graphene oxide using high-resolution in situ X-ray-based spectroscopies, J. Phys. Chem. C 115 (2011) 17009–17019.
[36] L.J. Cote, J. Kim, V.C. Tung, J.Y. Luo, F. Kim, Graphene oxide as surfactant sheets, Pure. Appl. Chem. 83 (2011) 95–110.
[37] N. Li, P.X. Zhao, D. Astruc, Anisotropic gold nanoparticles: synthesis, properties, applications, and toxicity, Angew. Chem. Int. Ed. 53 (2014) 1756–1789.
[38] D. Jana, C. Matti, J. He, L. Sagle, Capping agent-free gold nanostars show greatly increased versatility and sensitivity for biosensing, Anal. Chem. 87 (2015) 3964–3972.
[39] K.M. Mayer, J.H. Hafner, Localized surface plasmon resonance sensors, Chem. Rev. 111 (2011) 3828–3857.
[40] M. Li, S.K. Cushing, J. Zhang, J. Lankford, Z.P. Aguilar, D. Ma, N. Wu, Shape-dependent surface-enhanced Raman scattering in gold-Ramanprobe-silica sandwiched nanoparticles for biocompatible applications, Nanotechnology 23 (2012) 115501–115510.
[41] J. Zhang, Y. Sun, H. Zhang, B. Xu, H.Q. Zhang, D.Q. Song, Preparation and application of triangular silver nanoplates/chitosan composite in surface plasmon resonance biosensing, Anal. Chim. Acta 769 (2013) 114–120.
[42] A. Deep, A.L. Sharma, P. Kumar, L.M. Bharadwaj, Nanostructured polyaniline–silicon substrate for protein biosensing, Sens. Actuator B-Chem. 171–172 (2012) 210–215.
[43] Z.M. Liu, H.F. Yang, Y.F. Li, Y.L. Liu, G.L. Shen, R.Q. Yu, Core–shell magnetic nanoparticles applied for immobilization of antibody on carbon paste electrode and amperometric immunosensing, Sens. Actuator B Chem. 113 (2006) 956–962.
[44] J. Wang, D.Q. Song, H. Zhang, J. Zhang, Y. Jin, H.Q. Zhang, H. Zhou, Y. Sun, Studies of Fe_3O_4/Ag/Au composites for immunoassay based on surface plasmon resonance biosensor, Colloids Surf. B Biointer. 102 (2013) 165–170.
[45] J. Zhang, Y. Sun, Q. Wu, H. Zhang, Y. Bai, D.Q. Song, A protein A modified Au–graphene oxide composite as an enhanced sensing platform for SPR-based immunoassay, Analyst 138 (2013) 7175–7181.
[46] S. Shi, L.B. Wang, R.X. Su, B.S. Liu, R.L. Huang, W. Qi, Z.M. He, A polydopamine-modified optical fiber SPR biosensor using electroless-plated gold films for immunoassays, Biosens. Bioelectron. 74 (2015) 454–460.
[47] H. Zarei, H. Ghourchian, K. Eskandari, M. Zeinali, Magnetic nanocomposite of anti-human IgG/COOH–multiwalled carbon nanotubes/Fe_3O_4 as a platform for electrochemical immunoassay, Anal. Biochem. 421 (2012) 446–453.